Imaging of electron focusing in metallic single crystals

Abstract

The almost ballistic propagation of thermoelectrically excited carriers is investigated in single crystals using a real-space imaging technique. So-called electron focusing caustics, singularities of the carrier flux in real space, have been observed for the first time. These experiments allow to evaluate Fermi surfaces models and band structure calculations near the Fermi level. The influence of magnetic fields on the electron focusing patterns gives further information about the origin of the carriers.

1 Introduction

If the mean free path of carriers in metals becomes very large, i.e. in the range of several hundred μm, carriers can pass samples in this dimension without scattering. This is the so-called ballistic regime. To reach these large mean free paths experimentally, special conditions such as low temperatures and very pure and almost perfect crystals are necessary. Here, experiments using magnetic fields to focus electrons in metallic single crystals ([1], [2]) and also in semiconductor structures with two-dimensional electron systems [3] are of fundamental interest, since they probe nonclassical transport.

This report presents the application of a new technique for the investigation of ballistic transport of carriers in metals. Electrons and holes are excited thermoelectrically by local heating (Fig. 1). This is realized by illumination of a small point (hot spot) on one sample surface. If scattering processes are not dominant, the transport of the non-equilibrium carriers to the opposite sample surface may be highly anisotropic in relation to the Fermi surface geometry and the band-structure of the material. The carriers produce a current

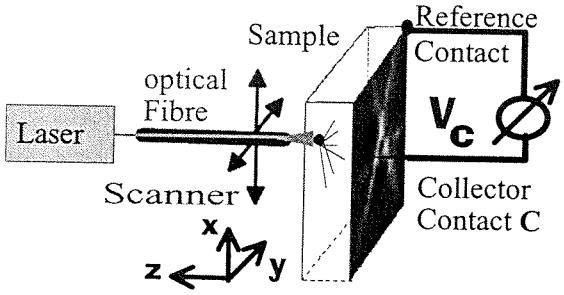

Fig. 1. Scheme of the experimental setup.

distribution which can be detected by a point contact at the other sample surface. Since the hot spot can easily be moved by a cryogenic micropositioning technique, this method allows real-space resolved measurements of ballistic transport. The detected patterns show the anisotropy of the electronic transport and can be interpreted as a kind of fingerprint of the Fermi surface of the material investigated in the experiment. Signals produced by electrons and holes can be distinguished by the application of a magnetic field.

2 Electron Focusing

In the case of ballistic propagation the carrier transport can be described by the first

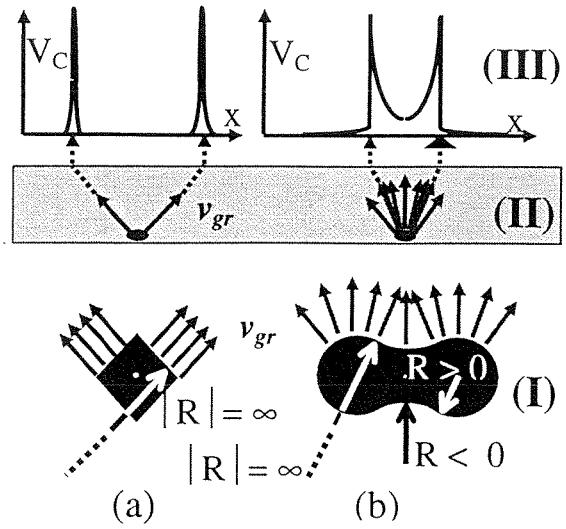

Fig. 2. The principle of electron focusing shown on two hypothetical examples in two-dimensional space: (I) Momentum space, (II) real space and (III) signal intensity. (a) Square and (b) "dog's bone".

equation of the semiclassical model of electronic motion: $\mathbf{v}_{gr} = \hbar^{-1}\nabla_k E(\mathbf{k})$. Here $\hbar = h/(2\pi)$, h is Planck's constant and k is the wave vector. This means that the group velocity vectors $\mathbf{v}_{gr}$ in real space (representing the spatial distribution of the electronic transport) are perpendicular to surfaces of constant energy $S_{E(\mathbf{k})}$ in k-space: $\mathbf{v}_{gr} \perp S_E$ (Fig. 2 (I)) . As the excited carriers have an energy distribution very close to the Fermi energy the consideration of exclusively Fermi electrons is a good approximation. The principle of electron focusing is shown in Fig. 2 on two hypothetical examples in two-dimensional space. In regions of very small or vanishing curvature of the Fermi-surfaces, i.e. infinite curvature radius (Fig. 2 (a) and (b)), the group velocity vectors (in real space) for neighboring k-states are (almost) parallel. This results in an enhancement of the carrier flux in real space (Fig. 2 (II)) along directions associated with regions of small or vanishing curvature of the Fermi surface in k-space. It can also be shown theoretically that the carrier flux intensity in real space related to a point on the Fermi surface is proportional to the product of the two principal curvature radii in this point [6]. Enhanced carrier transport due to a huge but not infinite curvature radius can be observed in the semimetal bismuth [4]. At a Fermi surface point with an infinite curvature radius the electronic flux in real space in the corresponding group velocity direction becomes singular. The occurrence of such singularities or "caustics" even in absence of a magnetic field are called electron focusing (EF)[4] in analogy to phonon focusing [5], the related phenomenon of highly anisotropic phonon transport. For the first time electron focusing was observed in the noble metal silver and later in the transition metal tungsten [8].

3 Setup

Fig. 1 (a) shows a scheme of the setup. An Ar-ion laser beam is chopped with a frequency $f \approx 100$ Hz and coupled into an optical fibre. Its end is brought $\approx 20\mu$m close to the sample surface. An area of $(\approx 20\mu\text{m})^2$ is illuminated with a power of ≈ 25 mW (hot spot). All experiments are performed in liquid ^{4}He at $T = 1.5$ K. The temperature difference between the cold crystal and the hot spot generates a thermal gradient and thus a thermoelectric current. To detect an EF-pattern the fibre is scanned over the surface by a cryogenic scanner [7]. The voltage v_C between the collector point contact C and a reference contact on the sample edge is detected as a function of the fibre position. This is equivalent to a fixed hot spot and a scanning collector contact, if the investigated crystal is homogeneous. As V_C is in the range of nV, phase sensitive detection is used. The samples were cut from single crystals by spark erosion to slabs of $d \approx 2$ mm thickness. The sample thickness was reduced to $\approx 0.35 - 0.5$ mm by etching or electrochemical polishing.

4 Results

4.1 The semimetal bismuth

Experimental results measured in a bismuth single crystal cut perpendicularly to the k_z- (trigonal) axis are shown in Fig. 3. V_C is presented in greyscale as a function of the fibre position. The electron signal appears brightly. Fig. 3 (a) shows threefold symmetry. The three bright lines forming a triangle originate from three extremely stretched electron ellipsoids of the Fermi surface of bismuth depicted in Fig. 3 (f). Increased electron flux occurs in planes perpendicular to the long half axes of the electron ellipsoids due to a vanishing Gaussian curvature. Since the ellipsoids are tilted about 6° out of the (k_x,k_y)-plane the planes with the sample surface opposite to the hot spot do not intersect in one point but leave a triangular void. The dark structures correspond to holes dragged by phonons. The result of Monte Carlo simulations using the bandstructure $E(k)$ of bismuth is shown in Fig. 3 (b). The anisotropic transport of ballistic carriers can be well described within the semiclassical model of electron dynamics. In order to investigate the influence of a magnetic field on the electron focusing-lines, a magnetic field $B_y = 0.3mT$ is applied in the y-direction. The line along the x-direction disappears, whereas the other two lines remain visible (Fig. 3 (c)). For $B_x = 0.4mT$ the situation is inverted (Fig. 3 (d)). If a magnetic field B_z=17 mT is applied in the z-direction a second set of lines appears. With increasing magnetic field the hole pattern shrinks together to a small point. For magnetic fields in the mT range the signal intensity oscillates with a constant period of B ≈5 mT due to the Sondheimer effect. For magnetic fields in the Tesla range so-called magnetooscillations periodic in B^{-1} can be observed [9].

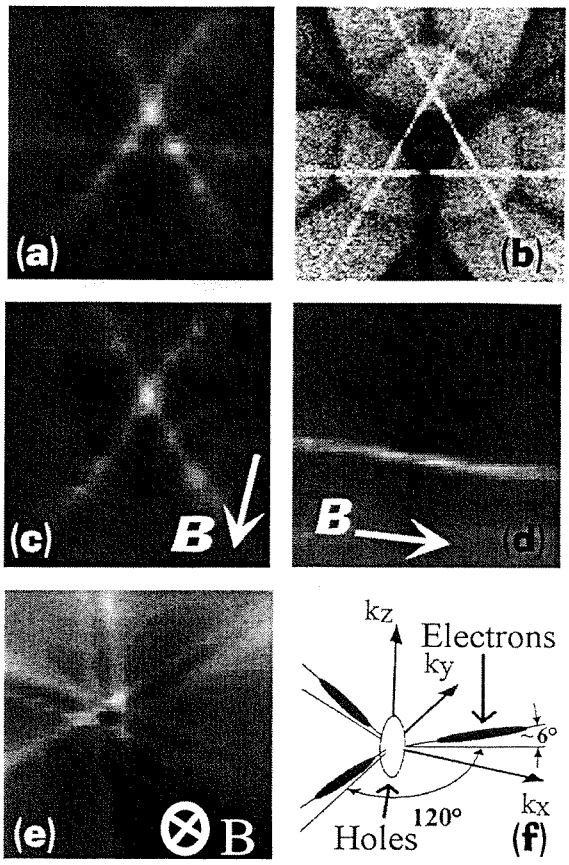

Fig. 3. Electron focusing in bismuth. (a) The voltage V_C is presented in greyscale as a function of the fibre position (40nV≤ V_C ≤160nV), the image frame is $(0.5\text{mm})^2$ and thickness of the crystal $d \approx 0.5$ mm. Holes dragged by phonons appear dark. (b) Theoretical focusing pattern (B=0). The electron focusing pattern is bright, the phonon focusing pattern (transverse 1 mode) is dark. (b) Same as (a) but $B_y = 0.3mT$. (c) Same as (a) but B_x= 0.4mT; the image frame is ≈ $(1\text{mm})^2$ and d≈0.5mm. (d) same as (a), but a longitudinal magnetic field of B_z=17mT is applied in the z-direction. (f) Fermi surface of bismuth.

4.2 The noble metal silver

A 100nm-CuNi layer was sputtered on one surface of a silver [110]-crystal to improve light absorption. The experimental result is shown in Fig. 4 (a). Two curved bright electron caustics enclosing a bright field and bordered by dark lines are visible. The two caustics originate from regions of vanish-

ing Gaussian curvature of the Fermi surface around the necks (see Fig. 4 (d)). The Monte Carlo calculations using the band structure data of silver ([10]) show similar caustics (Fig. 4 (b)), if only Fermi electrons are taken into account. Assuming a temperature drop between the hot spot ($T = T_h$) and the cold crystal ($T = T_c$) with corresponding Fermi distribution functions $f_h(E)$ and $f_c(E)$, a thermoelectric current proportional to $f_h(E) - f_c(E)$ will flow. Electrons with the energy $E > E_{Fermi}$ will propagate from the hot spot into the crystal and a countercurrent of electrons with $E < E_{Fermi}$ will move in the opposite direction. Within this simple model of thermal excitation the contribution of different energy levels around E_{Fermi} to V_C can be calculated. The sum over all levels yields the focusing image shown in Fig. 4 (c). Although the main features of the measured pattern agree with the calculation qualitatively, the intensities differ from the experimental ones.

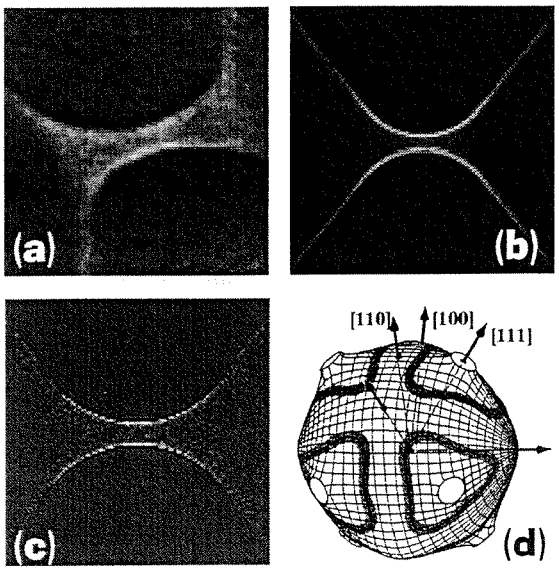

Fig. 4. Electron focusing in silver. (a) The voltage V_C is presented in greyscale as a function of the fibre position (0nV$\leq V_C \leq$2nV), the image frame is $(0.4\text{mm})^2$ and thickness of the crystal $d \approx 0.5$ mm. (b) Theoretical focusing pattern: only Fermi electrons are taken into account (frame size $(1.5d)^2$). (c) Theoretical focusing pattern for thermally excited electrons (frame size $(d)^2$). (e) Fermi surface of silver.

4.3 The transition-metal tungsten

Electron focusing patterns were detected for tungsten slabs cut perpendicularly to the [100], [110] and the [111]-direction (Fig. 5). The main contribution to the patterns is obviously produced by the hole octahedrons at the H-point of the Fermi surface (Fig. 5 (d)). The electron focusing pattern of the [110]-orientated sample (Fig. 5 (a)) shows two bright hole caustics. These two triangular rings are obviously caused by states with zero Gaussian curvature on the triangular faces of the hole octahedron (shaded in fig.5 (e)). The focusing pattern of the [100]-orientation (Fig. 5 (b)) shows four triangular caustics. They appear where the <111>-directions hit the surface. Since the <111>-directions enclose with the surface perpendicular to the [100]-direction an angle of about 55° the triangles are extremely strung-out. The dark spot in the center of the image is generated by electrons. Since the [111] pattern (Fig. 5 (d)) shows a "view" perpendicular to one octahedron face, the triangle is undistorted and centered in the pattern.

4.4 The superconductor niobium

In a niobium single crystals ring-like structures with an intensive peak in the middle have been observed under the influence of a longitudinal magnetic field of $B_z \approx 0.1T$ (Fig. 6 (a)). There are indications that the observed peak in the middle is somehow generated by excited quasiparticle states in the superconductor. It is assumed that the transport of the quasiparticles is going mainly ballistically between the vortices in the Shubnikov state. They are focused by the magnetic field in a way dependent on

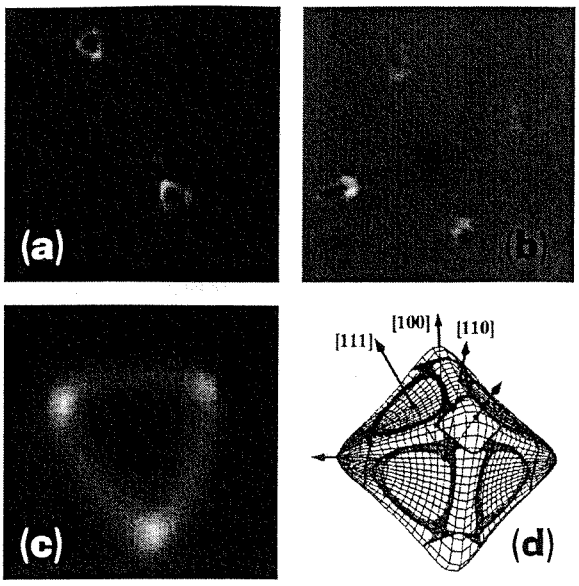

Fig. 5. Electron focusing in tungsten. The voltage V_C is presented in greyscale as a function of the fibre position, so that the hole signal appears brightly. (a) [110]-orientated ($0\text{nV} \leq V_C \leq 1.8\text{nV}$), the image frame is $(0.8\text{mm})^2$ and thickness of the crystal $d \approx 0.35$ mm. (b) [100]-orientated ($0\text{nV} \leq V_C \leq 0.61\text{nV}$), the image frame is $(0.6\text{mm})^2$ and thickness of the crystal $d \approx 0.35$ mm. (c) [111]-orientated ($0\text{nV} \leq V_C \leq 1.1\text{nV}$), the image frame is $(0.1\text{mm})^2$ and thickness of the crystal $d \approx 0.4$ mm. (e) Fermi surface of tungsten.

their effective charge. This may create the ringlike structures of the inner peak (Fig. 6 (b)).

5 Conclusions

We have presented a new experimental technique which is able to investigate nearly ballistic transport in metals. For the first time focusing of carriers originating from regions of small or vanishing curvature of the Fermi surface is clearly demonstrated. The detected patterns allow to test the validity of Fermi surface and band structure data. By a simple model the observed patterns can be simulated. Investigations in a magnetic field can provide supplementary information about the

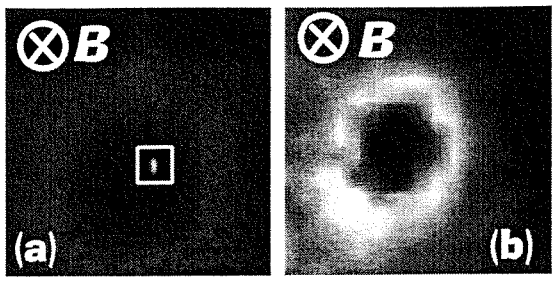

Fig. 6. Electron focusing in niobium in the vortex state: The voltage V_C is presented in greyscale as a function of the fibre position T=4.2K; B=0.1T; [110]-orientated; thickness of the crystal $d \approx 0.35$ mm; ($0\text{nV} \leq V_C \leq 18\text{nV}$). (a) The image frame is $(0.4\text{mm})^2$. (b) Zoom into (a), the image frame is $(130\ \mu\text{m})^2$.

origin of the carriers. The results presented here can be interpreted as the ballistic analogues of the Seebeck, Thomson, Hall or Nernst effect depending on the excitation method and the applied field. Besides thermal excitation and current injection other excitation methods (i.e. by an electron beam, by a tunneling contact or by ultrasonic waves) are conceivable or already realized ([11]). These new methods may improve the resolution so that other kinds of materials (i.e. semiconductors) could be investigated.

A.Böhm[a], J.Heil[a,b], M.Primke[a,c], A.Gröger[a] and P.Wyder[a]

(a) Grenoble High Magnetic Field Lab. - BP 166 - 38042 Grenoble Cedex 9,
(b) Actual address: Leica Microscopie und Systeme GmbH, Ernst-Leitz-Straße, D-35578 Wetzlar,
(c) Actual address: Hewlett-Packard, Herrenberger Str. 130, D-71034 Böblingen

F. E. Schönherr, H. Wendel, H. Bender, J. Major, P.Keppler

MPI, Heisenbergstraße 1, D-70569 Stuttgart

References

[1] Yu. V. Sharvin and L.M.Fisher, Zh. Eksp. Theor. Fiz. Pis'ma Red. **1**,54 (1965)

[2] V.S. Tsoi J.Bass, and P.Wyder, Adv. Phys. **41**, 365 (1992)

[3] C.W.J. Beenacker and H. van Houten, Solid State Phys **44**,1[1991]

[4] J. Heil, M. Primke, K. U. Würz, P. Wyder, Phys. Rev. Lett. **74**, 146 (1995)

[5] J. P. Wolfe, Physics Today **48** (9), 34 (1995)

[6] A.M.Kosevich, Sov. J. Low Temp. Phys. **11**,611 (1985)

[7] J. Heil, A. Böhm, M. Primke, P. Wyder, Rev. Sci. Instrum. **67** (1),(1996)

[8] J. Heil, M. Primke, A.Böhm, J.Major, P.Keppler and P. Wyder, Phys. Rev. B **54** (4), 2280 (1996)

[9] M.Primke, J.Heil, A.Böhm, A. Gröger and P.Wyder, Phys. Rev. Lett. **79**, 4882 (1997)

[10] D. A. Papaconstantopoulos, *Handbook of the Band Structure of Elemental Solids*, Plenum Press, New York (1986)

[11] S.Knauth et al. (University of Leipzig), to be published